Longitudinal Magnetic Resonance Imaging in Asymptomatic *C9orf72* Mutation Carriers Distinguishes Phenoconverters to Amyotrophic Lateral Sclerosis or Amyotrophic Lateral Sclerosis With Frontotemporal Dementia

Kevin van Veenhuijzen, MD, Harold H.G. Tan, MD, Abram D. Nitert, MD, Michael A. van Es, MD, PhD, Jan H. Veldink, MD, PhD, Leonard H. van den Berg, MD, PhD,* and Henk-Jan Westeneng, MD, PhD*

Objective: We prospectively studied asymptomatic *C9orf72* mutation carriers, identifying those developing amyotrophic lateral sclerosis (ALS) or frontotemporal dementia (FTD).

Methods: We enrolled 56 asymptomatic family members (AFM) with a *C9orf72* mutation (AFM C9+), 132 non-carriers (AFM C9−), and 359 population-based controls. Using 3 T magnetic resonance imaging, we measured cortical thickness, gyrification, and subcortical volumes longitudinally. Linear mixed-effects models on non-converting AFM C9+ scans (n = 107) created a reference for these measurements, establishing individual atrophy patterns. Atrophy patterns from presymptomatic phenoconverters (n = 10 scans) served as a template for group comparisons and similarity assessments. Similarity with phenoconverters was quantified using Dice similarity coefficient (DSC) for cortical and Kullback–Leibler similarity (KLS) for subcortical measures. Using longitudinal similarity assessments, we predicted when participants would reach the average similarity level of phenoconverters at their first post-onset scan.

Results: Five AFM C9+ converted to ALS or ALS-FTD. Up to 6 years before symptoms, these phenoconverters exhibited significant atrophy in frontal, temporal, parietal, and cingulate cortex, along with smaller thalamus, hippocampus, and amygdala compared to other AFM C9+. Some non-converted AFM C9+ had high DSC and KLS, approaching values of phenoconverters, whereas others, along with AFM C9− and controls, had lower values. At age 80, we predicted 27.9% (95% confidence interval, 13.2–40.1%) of AFM C9+ and no AFM C9− would reach the same DSC as phenoconverters.

Interpretation: Distinctive atrophy patterns are visible years before symptom onset on presymptomatic scans of phenoconverters. Combining baseline and follow-up similarity measures may serve as a promising imaging biomarker for identifying those at risk of ALS or ALS-FTD.

ANN NEUROL 2025;97:281–295

View this article online at wileyonlinelibrary.com. DOI: 10.1002/ana.27116

Received Mar 15, 2024, and in revised form Oct 1, 2024. Accepted for publication Oct 5, 2024.

Address correspondence to Dr van den Berg, University Medical Center Utrecht, Department of Neurology (G03.228), Heidelberglaan 100, PO Box 85500, 3508 GA Utrecht, The Netherlands. E-mail: l.h.vandenberg@umcutrecht.nl

*These senior authors contributed equally.

From the Department of Neurology, UMC Utrecht Brain Center, University Medical Center Utrecht, Utrecht, The Netherlands

Additional supporting information can be found in the online version of this article.

© 2024 The Author(s). *Annals of Neurology* published by Wiley Periodicals LLC on behalf of American Neurological Association.
This is an open access article under the terms of the Creative Commons Attribution-NonCommercial-NoDerivs License, which permits use and distribution in any medium, provided the original work is properly cited, the use is non-commercial and no modifications or adaptations are made.

Amyotrophic lateral sclerosis (ALS) and frontotemporal dementia (FTD) are neurodegenerative diseases associated with accumulation of proteinaceous intracellular inclusions.[1] ALS is characterized by degeneration of upper and lower motor neurons, causing progressive muscle weakness, respiratory insufficiency, and eventually death. FTD is characterized by degeneration of neurons in the frontal and temporal lobes, leading to behavioral and cognitive deficits. There is substantial overlap between the two diseases: up to 50% of ALS patients exhibit some degree of cognitive or behavioral impairment, and approximately 40% of FTD patients display signs of motor neuron disease.[1,2] Moreover, in separate cohort studies of the two diseases, approximately 15% of cases meet the diagnostic criteria for ALS-FTD.[1,2]

A GGGGCC hexanucleotide repeat expansion in *C9orf72* has been identified as the most common genetic mutation associated with both ALS and FTD, accounting for up to 44% of familial and approximately 6% of apparent sporadic ALS, and 25% of familial and 5% of sporadic FTD cases of European ancestry worldwide.[1–3] The penetrance for ALS is incomplete, with latest estimates varying widely between families and populations, averaging between 24 and 44%.[4,5] The exact penetrance for FTD is currently unknown. Predicting disease development solely through gene carriership is, therefore, insufficient. Currently, an increasing number of therapeutic options for *C9orf72*-associated ALS are being developed.[6] Considering the evidence that neurodegeneration occurs decades before symptom onset,[7] it may become feasible to initiate therapy during the presymptomatic phase.

Our objectives were to give a detailed longitudinal description of cerebral changes in phenoconverters in vivo using structural brain magnetic resonance imaging (MRI) to identify unique patterns that could serve as an early biomarker, potentially years before symptom onset, and therefore, differentiate asymptomatic individuals at high risk of developing ALS-FTD from those with a low risk.

Materials and Methods

Study Participants

For this ongoing longitudinal cohort study, 188 asymptomatic family members (AFM) of ALS or FTD patients with a mutation in *C9orf72* were enrolled at the University Medical Center Utrecht between 2010 and 2023. Methods of enrollment are detailed in previous research.[8] Asymptomatic was defined as lacking clinical signs of motor neuron disease, bulbar dysfunction, and behavioral and cognitive changes during the study. We tested for a pathological repeat expansion in *C9orf72* (C9+) in genomic DNA samples as described previously.[9] As recent research suggests that first- and second-degree relatives of ALS patients might be prone to cognitive and neuropsychiatric impairments, regardless of mutation status,[10] we also included 359 population-based healthy individuals ("controls") from the Dutch neuromuscular biobank.[11] Participants underwent standardized neurological examinations at every visit, as detailed previously.[12] Phenoconversion to clinically apparent ALS or FTD, according to the revised El Escorial and Rascovsky criteria,[13,14] was monitored, allowing stratification of the baseline AFM C9+ into phenoconverters and non-converting AFM C9+. In cases where data was initially incomplete, participants were promptly contacted to ensure comprehensive data capture. Hence, data collection was complete for all visits and no information was missing. Follow-up visits occurred after approximately 1 year and then every 5 years for asymptomatic subjects, and every 3 to 6 months for phenoconverters, for a total of 5 visits after symptom onset, or for as long as they were physically able to do so safely. As this study is part of a larger, ongoing investigation, the number of completed visits may differ between subjects depending on whether or not the individual's next scan interval had been reached. This variation does not necessarily indicate exclusion or loss to follow-up. This study was approved by the medical-ethical committee of the University Medical Center Utrecht. Written informed consent was obtained from all participants.

Acquisition and Preprocessing of Imaging Data

We used two 3T Philips (Best, The Netherlands) Achieva Medical Scanners to acquire T1 weighted images, following previously established parameters and preprocessing methods.[15] The two MRI scanners were identical in model and magnetic field strength. Scans were processed using FreeSurfer v7.3, measuring cortical thickness, local gyrification index (LGI) and deep gray matter volumes as described in earlier work.[8] Cortical thickness was assessed at 163,842 vertices per hemisphere, with all scans resampled to a common space for vertex-wise comparisons. Values were smoothed using a 10mm full-width half-maximum. We ensured the quality of both the unprocessed and processed images through qualitative inspection via manual review and quantitative assessment using the quality assurance tool integrated into the FreeSurfer software.

Subsegmentation of Subcortical Structures

Total volumes of deep gray matter structures, ventricles, and estimated total intracranial volume were retrieved from each subject. The thalamus was segmented into subregions using Bayesian inference, based on a probabilistic atlas developed using histological data. These subregions were merged into ten groups of nuclei with distinct physiological functions[16] (merged nuclei between brackets, if applicable): anteroventral, laterodorsal, lateral posterior, motor (ventral anterior, ventral anterior magnocellular, ventral lateral anterior, ventral lateral posterior), sensory (ventral posterolateral, ventromedial), intralaminar (central medial, central lateral, paracentral, centromedian, and parafascicular), medial (mediodorsal medial magnocellular, mediodorsal lateral parvocellular, reuniens, and paratenial), lateral geniculate, medial geniculate, and pulvinar (pulvinar pars anterior, medial, lateral and inferior, and limitans/suprageniculate). The hippocampus was segmented into twelve histologically

defined subfields[17]: parasubiculum, presubiculum, subiculum, CA1, CA2/3, CA4, granule cell layer of the dentate gyrus, hippocampal–amygdala transition area, fimbria, molecular layer, hippocampal fissure, and hippocampal tail. Last, the amygdala was divided into nine subregions based on histological data[18]: anterior amygdaloid area, cortico-amygdaloid transition, lateral nucleus, basal nucleus, accessory basal nucleus, paralaminar nucleus, medial nucleus, central nucleus, and cortical nucleus. Raw volume estimates of the above structures and their subsegmentations were all averaged between left and right.

Identification of Atrophy Patterns

Using scans of all non-converting AFM C9+, a linear mixed-effects model was fitted on each vertex to predict cortical thickness, and each subcortical structure to predict volume. We incorporated magnetic resonance (MR) scanner, age at imaging and sex as fixed effects, adding estimated total intracranial volume for the volumetric estimations. Participant pedigrees were converted to kinship matrices and used as covariance matrix of random effects to incorporate genetic relationships within the analyzed families. Subject identification (ID) was used as random intercept to model longitudinal measurements. These models were used as a reference to calculate residuals for individual scans within the other participant groups. To compute residuals for the individual non-converting AFM C9+ subjects, we used a leave-one-out approach, excluding the subject from the training set.[19]

To identify clusters of cortical atrophy or thickening (reflected by either negative or positive residuals) within a scan, we applied threshold free cluster enhancement (TFCE).[20] TFCE addresses the limitations of traditional cluster-based analysis methods by eliminating the need for arbitrary threshold selection. It also minimizes the probability of overfitting across all vertices by combining vertices into clusters. We assessed significance through permutation testing, comparing the TFCE-transformed cluster statistics with those generated through 1,000 permutations (each iteration reshuffling the residual value assigned to a random vertex). A p-value <0.05 was considered statistically significant. Vertices containing TFCE-transformed values not reaching significance were nullified. Cluster "weights" were calculated by summing TFCE-transformed values per cluster, with negative weights for negative clusters and vice versa. A control null distribution, representing cortical thickness variance in the general population, was derived from all cluster weights within control subjects' scans. Clusters were deemed significantly atrophied if their negative weight fell below the 2.5th percentile of the control null distribution, whereas clusters with a positive weight exceeding the 97.5th percentile were regarded significantly thickened.

Similarity between Phenoconverters and Other Groups

The atrophy pattern observed in presymptomatic phenoconverters was averaged based on the frequency of each vertex's inclusion in clusters identified with TFCE. This average pattern served as a mask for comparisons with other subject groups. We used a weighted Dice similarity coefficient (DSC),[21] ranging from 0 (no similarity) to 1 (exact copy), to determine the similarity between this mask and atrophy clusters in individual scans of each participant. The weighting considered the frequency at which a vertex was part of the affected clusters in the presymptomatic scans of phenoconverters.

Subcortical measurements were normalized across all scans using Z-transformation per structure. We applied the previously described mixed-effects model to each scan, calculating residuals per subcortical structure to construct a distribution of volume changes for each scan. We averaged the distributions resulting from presymptomatic scans of phenoconverters to describe the average pattern of subcortical volume changes in presymptomatic-phase phenoconverters. Similarity between each individual distribution and this average pattern was quantified by calculating the Kullback–Leibler divergence.[22] To align this outcome measure with DSC, we applied an inverse exponential transformation to have these values range from 0 to 1 and reflect similarity rather than dissimilarity.

We opted to use both DSC and transformed KLS because of their analogous operation, relying on pattern recognition with penalties for dissimilarity beyond the relevant area. DSC is traditionally used in medical imaging for evaluating the similarity of segmented regions, whereas Kullback–Leibler divergence is used in fields such as machine learning for model or graph comparisons. Both approaches mitigate the risk of individuals with diffuse atrophy or other similar conditions receiving inflated scores solely because of their pronounced deviation from the norm.

Statistical Analysis

We made pairwise comparisons in structural brain measurements with AFM C9− for presymptomatic phenoconverters, non-converting AFM C9+ and controls. Additionally, we compared non-converting AFM C9+ with presymptomatic phenoconverters to identify potential distinguishing features before symptom onset. We analyzed cortical thickness and subcortical volumes using linear mixed-effects models; LGI was analyzed using a non-linear mixed-effects model because of its negative logarithmic curve with ageing.[23] These models had the same fixed and random effects as described in a previous paragraph. In longitudinal analyses, age was added as random slope. For the cortical analyses, we will refer to the region within the previously described cortical atrophy cluster as "susceptible region", and the remainder as "resistant region." Interaction terms (subject group × region) were added to assess differential behavior per region across groups, and for longitudinal analyses, an "age × subject group × region" interaction was included. We used two-tailed statistical tests and p-values <0.05 were considered significant. We applied false discovery rate (FDR) correction to correct for multiple testing for subcortical volumetric analyses, with statistical significance set at p_{FDR} <0.05.

DSC and Kullback–Leibler similarity (KLS) were calculated for every scan using the previously described approach. The relationship between DSC and cortical thickness could best be described with a quadratic formula, where DSC was the dependent variable, age at imaging the fixed effect, region × DSC^2 the

interaction term, subject ID as random intercept and kinship as a covariance matrix of random effects. We used longitudinal DSC and KLS data to calculate individual annual changes during follow-up by incorporating age at imaging as random slope in the linear mixed-effects model. With this model, we predicted the age at which an AFM C9+, AFM C9− or control participant would have the same DSC or KLS as seen on average in the first scan made of phenoconverters after symptom onset. Confidence intervals for predicted onset ages were derived via bootstrapping (n = 10,000 simulations).

Sensitivity Analysis

In our efforts to minimize genetic influence on brain morphology, we added kinship to our models and used population-based controls to further minimize any physiological between-subject variance unaccounted for. To ensure that this did not introduce bias, we have added a sensitivity analysis the procedure was repeated for phenoconverters, but without kinship as a covariance matrix of random effects for our models.

For our predictive models regarding the estimated age at which a certain DSC or KLS value is reached, we assume that this value represents the period of phenoconversion to ALS. Given that these analyses are based on the relatively limited number of five subjects (with 20 scans) who phenoconverted, the inclusion of an additional phenoconverter with a markedly different pattern could potentially alter our findings significantly. To address this, we conducted the same analyses to calculate DSC for ALS C9+ patients at their first available scan after symptom onset. This allowed us to assert more confidently that these values are representative of phenoconversion.

Results

Demographics and Characteristics

Of the 188 enrolled family members, 56 were C9+. All were asymptomatic when enrolled, but four participants phenoconverted to ALS and one to FTD. The latter was also diagnosed with ALS, approximately 2.5 years after his diagnosis of FTD. On average, these five subjects were diagnosed after 59 months of follow-up (median, interquartile range [IQR] = 14–63 months). Three of the five phenoconverters (60%) debuted with a spinal onset, one (20%) with bulbar symptoms and one (20%) with cognitive and behavioral changes. The latter also developed spinal motor symptoms approximately two years later. The first affected limb was different between all subjects. Demographic details for all participants can be found in Table 1, with a Venn diagram in Figure S1. providing a graphical representation of the imaging data available for the asymptomatically enrolled C9+ subject subgroups. Additional clinical characteristics of the phenoconverters are listed in Table 2.

Three AFM C9− and two AFM C9+ individuals missed follow-up visits because of claustrophobia. Two AFM C9− participants passed away (unrelated to ALS). Three AFM C9− and one AFM C9+ were excluded from follow-up because of developing structural brain anomalies (eg, stroke, tumor). Four AFM C9− and one AFM C9+ had visits discontinued because of physical challenges. Nine AFM C9− and two AFM C9+ were lost to follow-up. Four of the five phenoconverters discontinued participation in MRI research because of physical fitness limitations caused by ALS; the remaining on emigrated to another continent.

Distinct Cortical Atrophy Pattern in Phenoconverters

Phenoconverters displayed a pattern of significant cortical atrophy compared to non-converting AFM C9+ (Fig 1). This pattern was already detectable in the first available scan of each phenoconverter, up to six years before symptom onset, and the area of the regions involved expanded through time. We found no distinguishable clusters of thicker cortex in phenoconverters. In our sensitivity analysis, where we repeated the procedure without including kinship in the models, we observed that the same brain regions were generally affected, but in a more diffuse manner (Fig S2.).

Figure 2 depicts the average pattern of cortical atrophy that distinguishes presymptomatic phenoconverters from non-converting AFM C9+ (ie, the "susceptible region"). This susceptible region comprises parts of the precentral, paracentral, superior frontal, caudal middle frontal, inferior frontal, lateral and medial orbitofrontal, superior, middle and inferior temporal, supramarginal, precuneus, and cingulate gyrus.

Cortical Thickness in the Susceptible Region

Cortex in the susceptible region was significantly thinner in presymptomatic phenoconverters than in non-converting AFM C9+ ($p < 0.001$) (Fig 3A). When compared to the resistant region, the susceptible region was significantly thicker across all subject groups ($p < 0.001$) (Fig 3A). There were no differences in cortical thickness between presymptomatic phenoconverters and non-converting AFM C9+ in the resistant region. Cortical thickness did not differ between AFM C9− and controls.

Longitudinally, cortical thinning was significantly faster in the susceptible region than in the resistant region for all subjects ($p < 0.001$) (Fig 3B). The rate of cortical thinning did not differ significantly between presymptomatic phenoconverters and non-converting AFM C9+, nor were there differences in cortical thinning between controls and AFM C9− (Fig 3B).

To maintain clarity, only the adjusted means of cortical thickness are displayed in the figures. Raw data, presented as scatter plots, can be viewed together with these estimations in Figure S3.

TABLE 1. Cohort Characteristics

	AFM C9+					
	Phenoconverters		Non-converting AFM C9+	AFM C9–	Controls	ALS C9+
	Presymptomatic phase	Symptomatic phase (ALS/FTD)				
Subjects, n	5		51	132	359	59
Sex, male	4 (80.0)		22 (43.1)	62 (47.0)	247 (68.8)	40 (67.8)
Handedness, right	4 (80.0)		46 (90.2)	116 (87.9)	324 (90.3)	49 (83.1)
Age at first scan, yr	58.5 (51.7–60.3)	60.7 (55.4–60.3)	43.4 (31.4–54.7)	46.9 (30.6–58.5)	62.9 (55.5–69.0)	59.6 (52.1–65.3)
Follow-up, mo	58.9[a] (14.3–63.0)	11.3[b] (10.5–15.6)	21.3 (14.2–77.9)	21.3 (13.7–76.5)	–	–
Disease duration, mo	–	10.5[c] (8.7–11.3)	–	–	–	16.5 (11.3–21.1)
Scans per visit, n						
Visit 1	5	–	51	132	359	59
Visit 2	5	–	38	90	–	–
Visit 3	–	5	17	48	–	–
Visit 4	–	3	1	–	–	–
Visit 5	–	2	–	–	–	–
Total scans, n	20		107	270	359	59

Data are shown as median (IQR) and count (%).
[a]From enrolment to symptom onset.
[b]Starting from symptom onset.
[c]At first scan after symptom onset.
Abbreviations: AFM = asymptomatic family member at enrolment; ALS = amyotrophic lateral sclerosis; C9+ = carrier of a pathogenic *C9orf72* repeat expansion; C9– = no pathogenic *C9orf72* repeat expansion; mo = months; yr = year.

Gyrification of the Susceptible Region

For all participants, LGI was significantly higher in the susceptible region than in the resistant region ($p < 0.001$). For both presymptomatic-phase phenoconverters and non-converting AFM C9+, we found no evidence that LGI was relatively more or less affected in the susceptible

TABLE 2. Phenoconverter Case Descriptions

Case	Sex	Age at onset[a]	First scan to symptom onset[b]	Symptoms of onset	Survival[c]
1	Male	61	14	Loss of fine motor skills and weakness in both arms	27
2	Female	70	63	Weakness in right leg	36
3	Male	44	59	Loss of fine motor skills and atrophy left arm	23
4	Male	58	68	Dysarthria and dysphagia	17
5	Male	53	4	Cognitive and behavioral changes	>72[d]

[a]In years.
[b]In months. Presented values were rounded to ensure privacy of the participant.
[c]Since onset, in months. Presented values were rounded to ensure privacy of the participant.
[d]Subject is alive at time of writing.

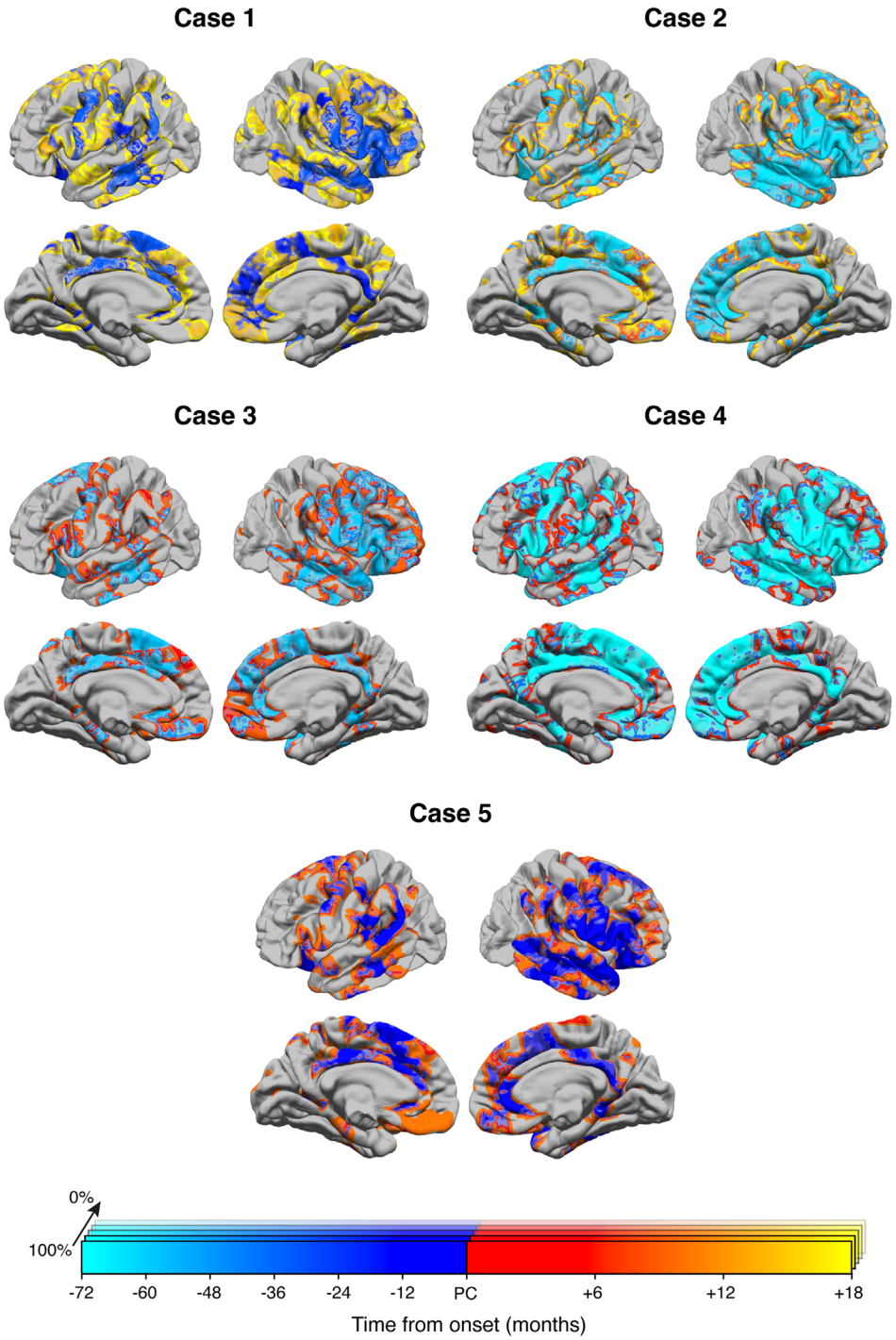

FIGURE 1: Individual cortical atrophy patterns in phenoconverters. For every case, scans are merged into one 3-dimensional brain image and color-coded for additional identified atrophy during later visits. Transparency (100 → 0%) is vertex overlap in subsequent scans of one individual. At the first scan during their presymptomatic phase, all phenoconverters displayed atrophy patterns discernible from non-converting asymptomatic family members carrying a pathogenic *C9orf72* repeat expansion. First scans were made: 14 months before symptom onset for case 1, 63 months for case 2, 59 months for case 3, 68 months for case 4, and 4 months for case 5. PC = phenoconversion.

region than in the resistant region (Fig 3C). No significant differences in LGI were observed between non-converting AFM C9+ and presymptomatic-phase phenoconverters, or between AFM C9− and controls.

Longitudinally, global LGI decreased with age in all groups ($p < 0.001$), and this decrease in LGI did not differ between the susceptible region and the resistant region (Fig 3D). Compared to non-converting AFM C9+, LGI

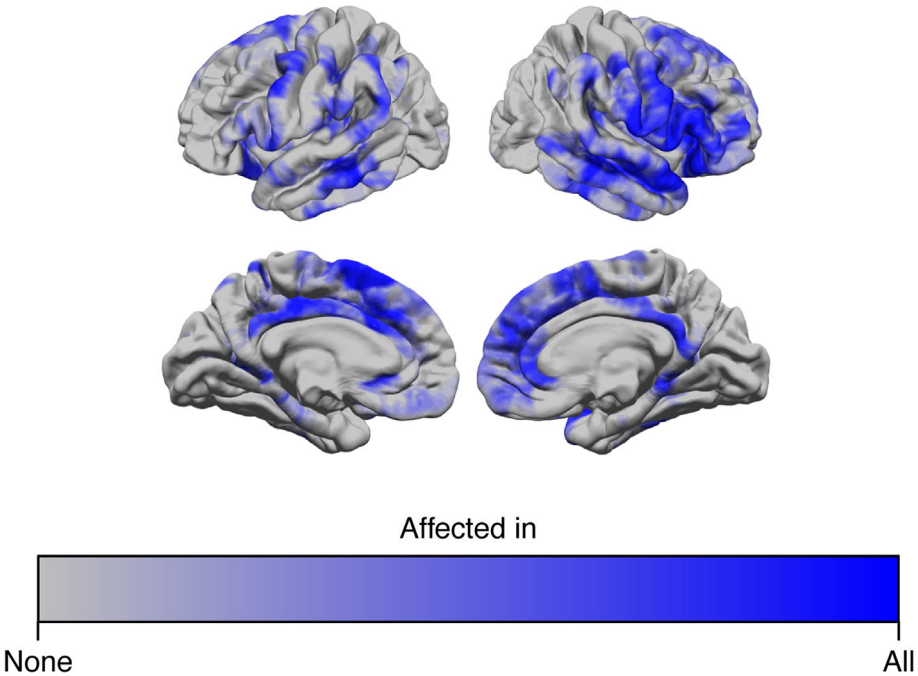

FIGURE 2: The susceptible region in presymptomatic phenoconverters. Average pattern of cortical atrophy in presymptomatic-phase phenoconverters compared to non-converting asymptomatic family members carrying a pathogenic *C9orf72* repeat expansion. Each vertex was colored according to the frequency with which it was found to be affected over all presymptomatic scans of phenoconverters. The non-involved part of the brain is called "resistant region."

decreased significantly faster in presymptomatic-phase phenoconverters ($p = 0.004$) (Fig 3D).

To ensure clarity, these figures display only the adjusted means. The raw LGI data, shown as scatter plots, can be found alongside these estimations in Figure S3.

Patterns of Subcortical Volume Changes in Phenoconverters

Group comparisons of deep gray matter structures and ventricles are presented in Table S1., with their average volume loss patterns visualized in Figure 4. Compared to AFM C9–, both non-converting AFM C9+ and presymptomatic phenoconverters had a significantly smaller thalamus, hippocampus, amygdala, and accumbens nucleus. Additionally, the pallidum was significantly smaller in presymptomatic phenoconverters, but not in non-converting AFM C9+. No significant differences in total subcortical structure volume were found between presymptomatic phenoconverters and non-converting AFM C9+, nor between AFM C9– and controls.

Subsegmentation of thalamus, hippocampus, and amygdala revealed numerous nuclei and subfields significantly smaller in both presymptomatic phenoconverters and non-converting AFM C9+ compared to AFM C9− (Table S1.). The lateral nucleus of the amygdala was more affected in presymptomatic phenoconverters than in non-converting AFM C9+ ($p_{FDR} = 0.017$). Other nuclei displayed the same trend, but p-values became non-significant after FDR correction.

Longitudinally, no significant differences were observed in volume reduction rates between presymptomatic phenoconverters and non-converting AFM C9+, nor between AFM C9− and controls.

Similarity with Phenoconverters' Cortical Atrophy Patterns

The DSC of the baseline scans of all participants is illustrated in Figure 5A. As one might expect, all five baseline scans of presymptomatic-phase phenoconverters have a high similarity to this pattern and tend to group together (mean $DSC_{baseline}$, 0.82; range, 0.60–0.95). Controls and AFM C9− have comparable low similarity; all 491 first scans having $DSC_{baseline} \leq 0.25$. Interestingly, non-converting AFM C9+ had more varying similarity in their baseline scans with the average presymptomatic-phase phenoconverter atrophy pattern: 20 scans had low DSC akin to the control groups with $DSC_{baseline} \leq 0.25$, three had high similarity surpassing the lower bound of presymptomatic phenoconverters at $DSC_{baseline} = 0.60$, and the remaining 28 scans had a moderate similarity with $DSC_{baseline}$ ranging from 0.25 to 0.60.

During follow-up, all presymptomatic phenoconverters had a high DSC_{slope} (mean, 0.021/year; range, 0.016–0.028), whereas all AFM C9− remained largely unchanged (mean DSC_{slope}, 0/year; range, −0.006 to 0.005). As with

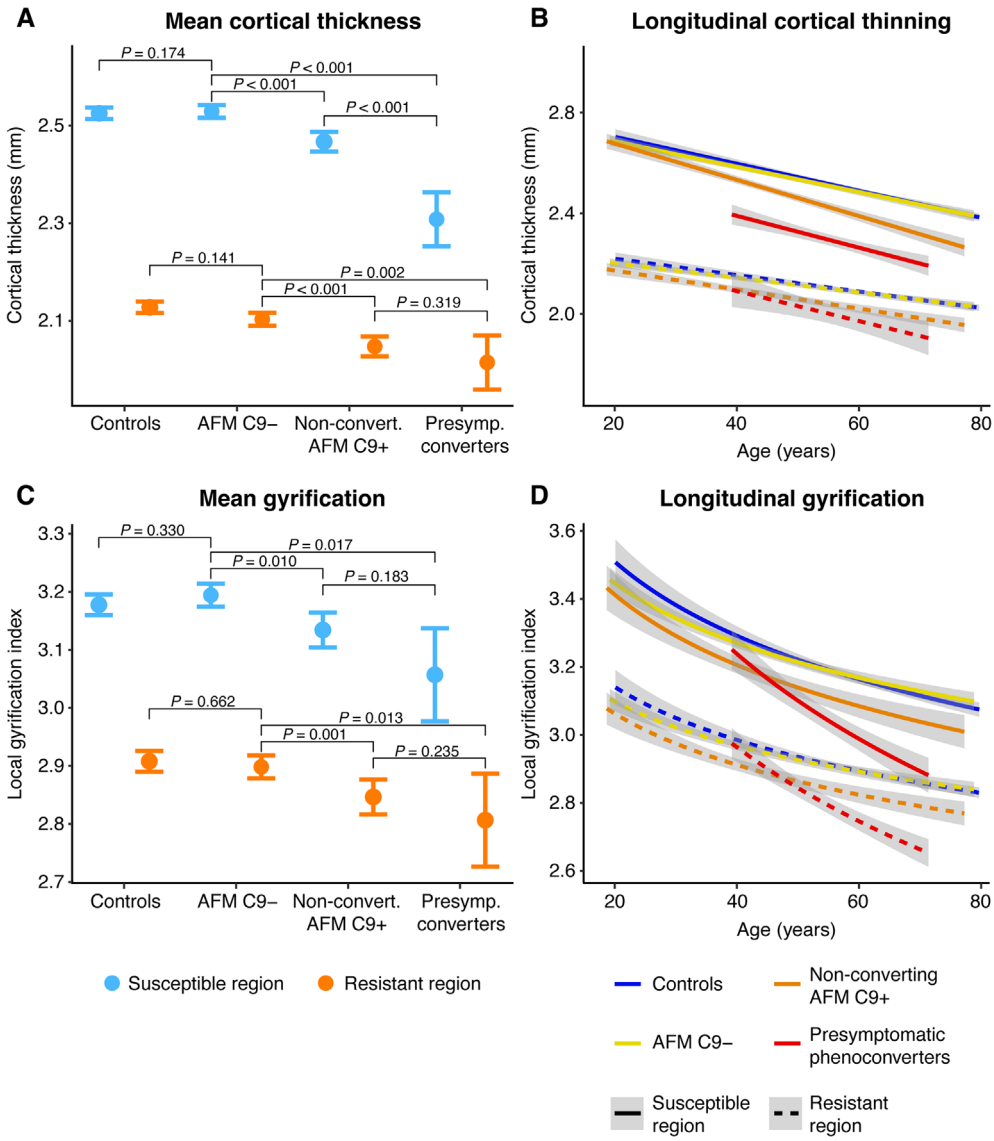

FIGURE 3: Groupwise comparisons of cortical measurements per brain region. Stratified as susceptible and resistant regions (see Fig 2). (A) Estimated marginal means of cortical thickness. (B) Longitudinal trajectories of cortical thickness and gyrification. (C) Estimated marginal means of gyrification. (D) Longitudinal trajectories of gyrification. Whiskers in A and C and gray ribbons in B and D represent 95% confidence intervals. AFM = asymptomatic family member; C9+ = carrier of a pathogenic *C9orf72* repeat expansion; C9– = no pathogenic *C9orf72* repeat expansion; Controls = unrelated population-based controls.

$DSC_{baseline}$, non-converting AFM C9+ had varying rates of annual changes in their similarity measures: ten had low DSC_{slope} (<0.005) like AFM C9−, three had a higher rate, surpassing the lower bound of presymptomatic phenoconverters ($DSC_{slope} = 0.016$), and the other 38 non-converting AFM C9+ had an intermediate DSC_{slope} ranging from 0.005 to 0.016 (Fig 5B). Controls were excluded from this analysis as they did not have follow-up scans.

Generally, there is a strong positive correlation between $DSC_{baseline}$ and DSC_{slope} (Pearson's $\rho = 0.75$, $p < 0.001$) (Fig 5C). Note, the three AFM C9+ with a high DSC_{slope} were not the same individuals as the three AFM C9+ with a high $DSC_{baseline}$. Therefore, it is apparent that there are some AFM C9+ with a much higher DSC_{slope} than explained by $DSC_{baseline}$. Regression models showed no significant relationship between follow-up time or age and either $DSC_{baseline}$ or DSC_{slope} (not visualized). We also found a significant (non-linear) negative correlation between DSC and cortical thickness ($p = 0.002$) (Fig 5D). This effect was stronger within the susceptible region than in the resistant region ($p < 0.001$).

Similarity with Phenoconverters' Subcortical Atrophy Patterns

All 5 presymptomatic phenoconverter baseline scans had high similarity, with mean $KLS_{baseline} = 0.79$ (range, 0.73–0.92). Unlike DSC, $KLS_{baseline}$ showed wide and overlapping distribution for controls, AFM C9− and non-

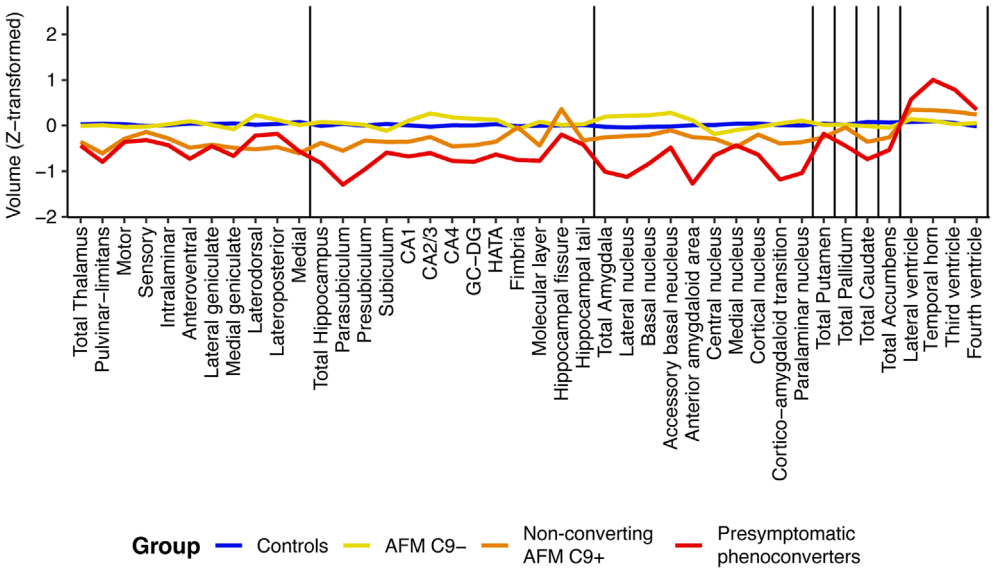

FIGURE 4: Patterns of volume loss per subcortical region. Volumes are Z-transformed for better inter-region comparison. AFM = asymptomatic family member; C9+ = carrier of a pathogenic *C9orf72* repeat expansion; C9– = no pathogenic *C9orf72* repeat expansion; CA = cornu ammonis; Controls = unrelated population-based controls; GC-DG = granule cell layer of the dentate gyrus; HATA = hippocampal–amygdala transition area.

converting AFM C9+ (Fig 6A). For controls, mean $KLS_{baseline}$ was 0.61 (range, 0.35–0.85), for AFM C9−, mean $KLS_{baseline}$ was also 0.61 (range, 0.40–0.88), and for AFM C9+, mean similarity measured slightly higher with $KLS_{baseline} = 0.64$ (range 0.47–0.86). On average, all groups displayed an annual increase in KLS, or KLS_{slope} (Fig 6B). This increase was highest in presymptomatic phenoconverters (mean, 0.019; range, 0.015–0.027), followed by AFM C9+ (mean, 0.006; range, − 0.013 to 0.021), and last AFM C9− (mean, 0.005; range, − 0.015 to 0.022). Overall, there is a strong positive correlation between $KLS_{baseline}$ and KLS_{slope} (Pearson's $\rho = 0.77$, $p < 0.001$) (Fig 6C). Regression models did not show a significant relationship between follow-up time or age and either $KLS_{baseline}$ or KLS_{slope} (not visualized). The correlation between KLS and DSC (Fig 6D) is low, indicating that cortical DSC and subcortical KLS measure two different aspects of the brain.

Predicting Age of Reaching Conversion Endophenotype

At first scan after symptom onset (median, 10.5 months; IQR, 8.7–11.3 months), mean DSC was 0.85 and mean KLS was 0.77. Estimated lifetime trajectories in DSC and KLS for each phenoconverter, extrapolated from their presymptomatic imaging data, are displayed in Figure 7A, B. For all phenoconverters, age at symptom onset was close to their predicted age of reaching DSC = 0.85 (median difference, −1.3 years; IQR, −4.9 to +1.6 years). However, for KLS, the median difference between age at symptom onset and predicted age of reaching KLS = 0.77 was larger at −7.9 years (IQR, −10.0 to −7.1 years), primarily because of 1 outlier (case 1, Fig 7B). Two examples of non-converting AFM C9+ are also illustrated in Figure 7A, B, where one has high $DSC/KLS_{baseline}$ and DSC/KLS_{slope} (red dashed line) and the other has low values (gray dashed line). Sensitivity analysis in 59 ALS C9+ showed that DSC at first scan after symptom onset (median, 16.5 months; IQR, 11.3–21.1 months) was comparable to that of the five phenoconverters with mean DSC = 0.80 (range, 0.57–0.97).

According to our predictions using DSC, at the age of 80 years, 27.9% (95% CI, 13.2–40.1%) of AFM C9+ are expected to have a cortical endophenotype similar to the DSC of the first scan of phenoconverters after symptom onset (Fig 7C). We estimated that none (95% CI, 0.0–0.0%) of the 132 AFM C9– studied would develop this endophenotype by age 80. Using KLS, a predicted 24.9% (95% CI, 10.8–36.7%) of mutation carriers at age 80 will have a subcortical endophenotype akin to phenoconverters soon after symptom onset, whereas in non-carriers this would be 4.3% (95% CI, 0.1–8.5%) (Fig 7D).

Discussion

In this prospective study, we used longitudinal high-resolution T1-weighted MRI scans in a large cohort of asymptomatic *C9orf72* mutation carriers to examine the cortical and subcortical structures of those individuals who

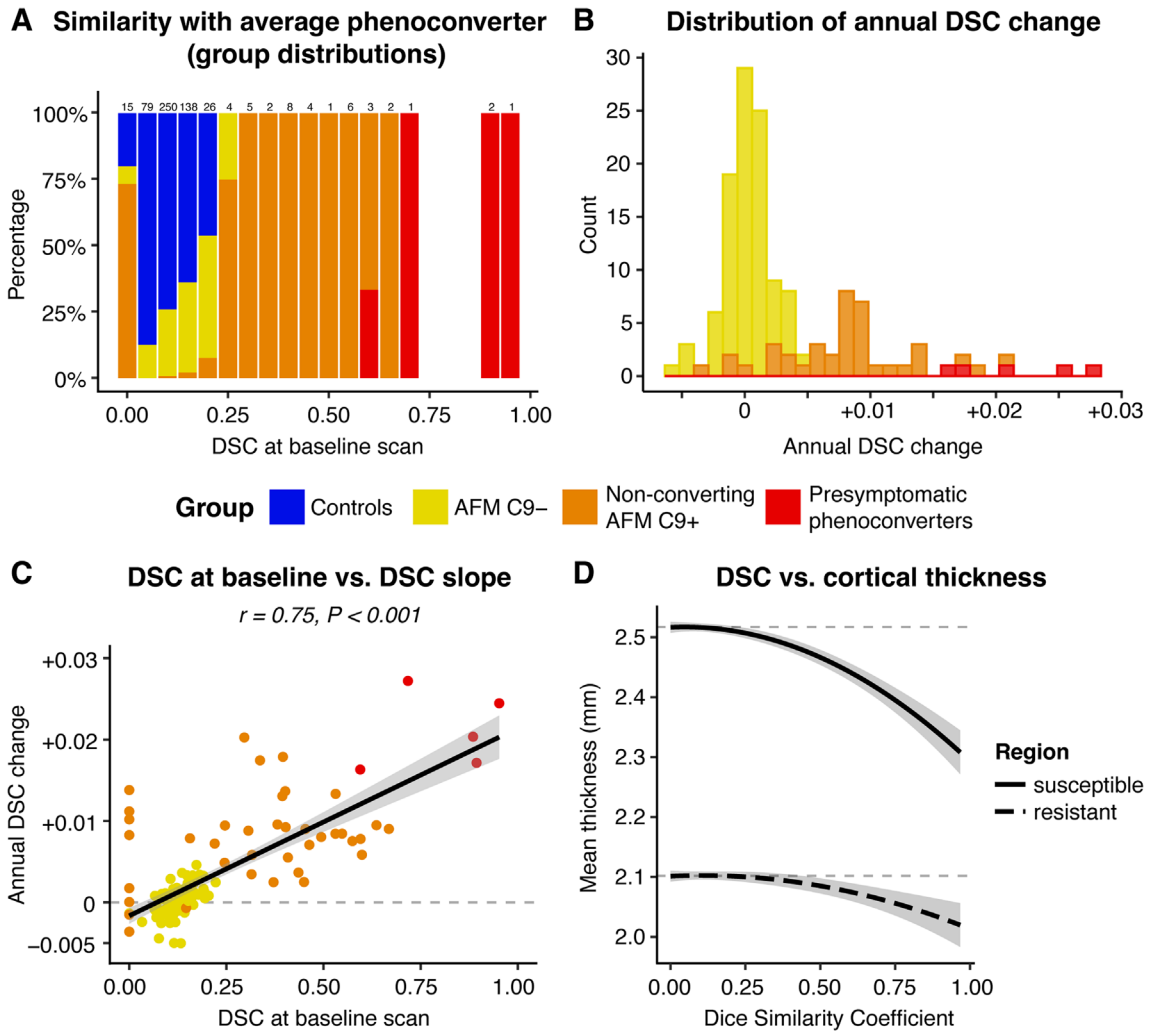

FIGURE 5: Cortical similarity with average presymptomatic phenoconverter magnetic resonance imaging. (A) Distribution of baseline DSC values stratified per subject group. Baseline was defined as the moment of first scan at enrolment. Values were binned at 0.05, and total of every bar is 100% (within each bin). n Subjects per value are indicated at the top of each bar. (B) Histogram of the annual change in DSC during follow-up, stratified per subject group. Controls are absent as they did not have any follow-up visits. (C) Correlation between baseline DSC and rate of annual change in DSC during follow-up. (D) Relationship between DSC and cortical thickness within all subjects, stratified by susceptible and resistant regions (see Fig 2). Gray ribbons in C and D represent 95% confidence intervals. AFM = asymptomatic family member; C9+ = carrier of a pathogenic *C9orf72* repeat expansion; C9– = no pathogenic *C9orf72* repeat expansion; Controls = unrelated population-based controls; DSC = Dice similarity coefficient.

converted to ALS or ALS-FTD. With models trained on scans of non-converting AFM C9+, we discovered consistent and distinct patterns of cortical thinning and subcortical volume loss in individual scans of presymptomatic phenoconverters. These patterns could already be detected in the earliest MRI scans performed years before symptom onset. For every participant, we quantified similarity of their scans with these patterns using DSC for cortical and KLS for subcortical measures. A subset of AFM C9+ exhibited high similarity with presymptomatic phenoconverters, and within the group of non-converting AFM C9+, there is notable variability in the annual change in this measure, unlike controls and AFM C9−. With these measures, we estimated that 27.9% of AFM C9+ may exhibit an endophenotype akin to phenoconverters by age 80. Overall, our results propose a potential new method to quantify presymptomatic disease progression and forecast the timing of clinically manifest phenoconversion.

Our findings in AFM C9+ demonstrate structural impairments consistent with previous radiological studies, revealing thinning in the frontal, temporal, parietal and cingulate cortex,[24–27] abnormal gyrification,[28] and volume loss in (subregions of) the thalamus, hippocampus, amygdala, caudate and putamen.[24,25,29,30] Although group comparisons between AFM C9+ and AFM C9− or unrelated controls provide insight into changes associated with gene mutation carriership during the asymptomatic phase, they do not discern whether they are linked to

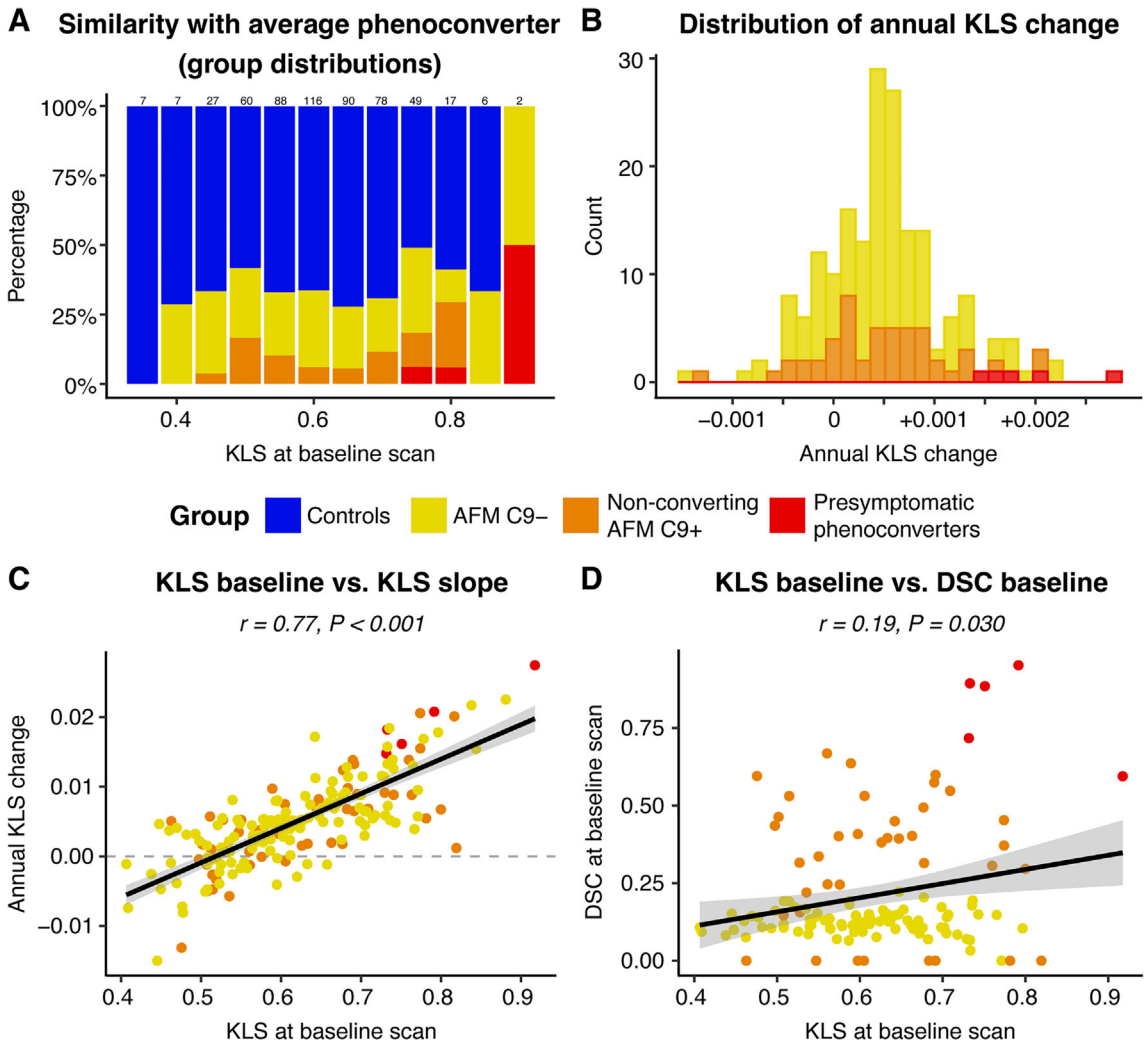

FIGURE 6: Subcortical similarity with average presymptomatic phenoconverter magnetic resonance imaging. (A) Distribution of baseline KLS values stratified per subject group. Baseline was defined as the moment of first scan at enrolment. Values were binned at 0.05, and total of every bar is 100% (within each bin). n Subjects per value are indicated at the top of each bar. (B) Histogram of the annual change in KLS during follow-up, stratified per subject group. Controls are absent as they did not have any follow-up visits. (C) Correlation between baseline KLS and rate of annual change in KLS during follow-up. (D) Correlation between cortical DSC and subcortical KLS at baseline. Gray ribbons in C and D represent 95% confidence intervals. AFM = asymptomatic family member; C9+ = carrier of a pathogenic *C9orf72* repeat expansion; C9− = no pathogenic *C9orf72* repeat expansion; Controls = unrelated population-based controls; DSC = Dice similarity coefficient; KLS = Kullback–Leibler similarity.

imminent symptom onset or merely indicate disease susceptibility. To make this distinction, longitudinal assessments in AFM C9+, who eventually develop clinically manifest disease, are critical. Until now, however, no such ALS imaging studies have been published. For familial FTD, imaging studies have been conducted on a cohort of phenoconverted GRN and MAPT mutation carriers.[31–33] Analogous to our work, they found that phenoconverters could be distinguished from non-converters using classification scores based on multimodal imaging techniques. Unlike our study, presymptomatic GRN and MAPT mutation carriers did not show distinguishing features more than two years before symptom onset. This might be because of differences in the mutations carried[34] or variations in the pathophysiology between FTD and ALS-FTD. Another explanation could be the differences in methodologies, such as our use of atrophy patterns or incorporating kinship in our statistical models, which addresses potential confounding by shared genetic factors and enhances statistical power.

Notably, the MRI scans of the ALS-FTD case showed high comparability in atrophy pattern with the average of the other four phenoconverters (DSC ≈ 0.85), despite his cognitive/behavioral onset as opposed to the others' motor symptom onset. This subject developed ALS approximately 2.5 years after developing FTD. Based

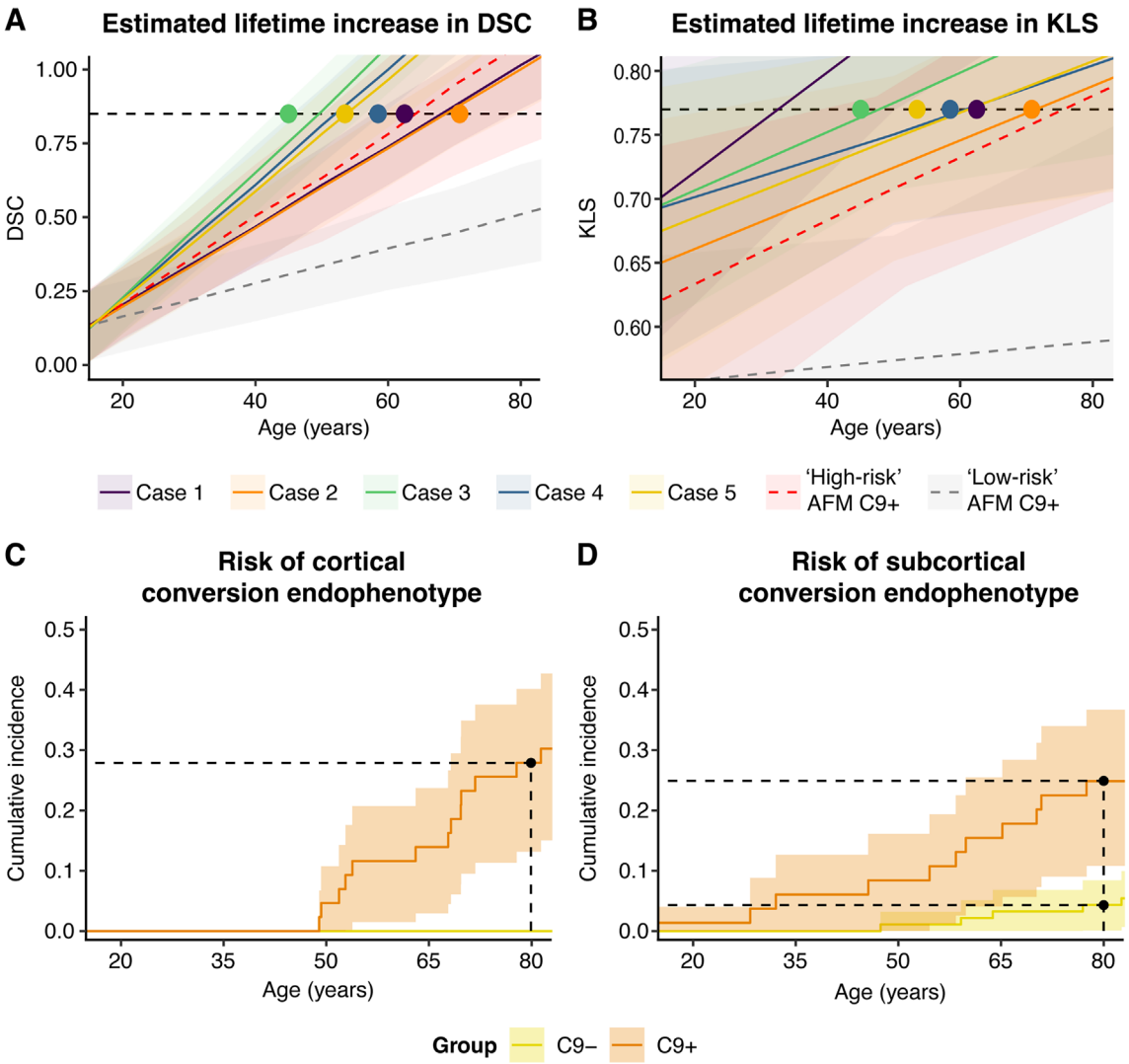

FIGURE 7: Predictions in lifetime DSC and KLS trajectories. (A) Predicted change in DSC and (B) predicted change in KLS during life in phenoconverter cases (solid lines) and two examples of non-converting AFM C9+ (dashed line). A "high risk" AFM C9+ had high DSC or KLS at baseline, and a high slope during follow-up (both higher than lower bound of phenoconverters), whereas these were both low for "low risk" AFM C9+. The dashed horizontal line is the average value of phenoconverters at their first visit after symptom onset (DSC = 0.85, KLS = 0.77). The dots represent the age at symptom onset. (C) Predicted cumulative incidence curve of developing a cortical endophenotype similar to the first scan after symptom onset in phenoconverters (DSC = 0.85). (D) Predicted cumulative incidence curve of developing a subcortical endophenotype similar to the first scan after symptom onset in phenoconverters (KLS = 0.77). Subjects are grouped by genotype. The black dashed horizontal line marks the predicted cumulative incidence at age 80. The shaded areas represent the bootstrapped 95% confidence interval (10,000 simulations). AFM = asymptomatic family member; C9+ = carrier of a pathogenic *C9orf72* repeat expansion; C9– = no pathogenic *C9orf72* repeat expansion; DSC = Dice similarity coefficient; KLS = Kullback–Leibler similarity.

on our current information, we cannot definitively determine whether there is a distinct pattern difference between ALS and FTD. Hypothetically, it is possible that the observed atrophy pattern in the ALS-FTD case primarily reflects ALS, especially because this pattern is also visible several years before developing ALS in the other cases. Moreover, this pattern is consistent among all 20 scans of the five phenoconverters, despite considerable sources of variance such as gender, age at onset, or location of first symptoms. This suggests that the identified pattern associated with ALS is largely unrelated to clinical heterogeneity.

This study explored the utility of both DSC and KLS in discriminating phenoconverters from AFM C9+ and predicting the emergence of an endophenotype akin to phenoconverters shortly after symptom onset. In this context, DSC demonstrated better performance than KLS. A possible application of these measures could be to identify asymptomatic individuals at elevated risk for developing ALS or ALS-FTD. For example, individuals with an intermediate to high baseline DSC and a relatively steep DSC slope (eg, >0.25 and >0.01/year, respectively) might be considered at higher risk, whereas those with low

baseline DSC or slope may tentatively be classified as low-risk. This might be of use, for instance, in enrolment criteria for presymptomatic trials for ALS or ALS-FTD. In addition to their potential use as a marker for predicting impending symptomatology, DSC or KLS could also be explored for evaluating treatment effects of (presymptomatic) therapies in trials. For instance, in the treatment of conditions like multiple sclerosis, "No Evidence of Disease Activity" (which is partly based on MRI findings) is also used as a primary or secondary endpoint to assess treatment effectiveness.[35] This would add a non-invasive method for monitoring treatment effect, potentially offering greater specificity compared to measuring serum or cerebrospinal fluid levels of neurofilaments. Before implementation, this warrants further international research to replicate and validate our findings in longitudinal studies that have assessed phenoconverters during their presymptomatic and symptomatic phases. Preferably, this research would encompass various genetic mutations and be conducted in collaboration with research groups investigating FTD families.

Monitoring of neurofilaments has gained prominence, given their rise above normative thresholds preceding clinically manifest ALS or FTD, occurring within a range from three years before to a few months after emergence of clinically manifest disease.[36–38] Despite this advance, a potential limitation lies in the relatively short window for predicting disease onset, necessitating frequent testing. Furthermore, to halt or prevent the process of neurodegeneration as far as possible, it is imperative to start treatment before large-scale axonal damage occurs (which is measured with increasing NfL). The distinct atrophy patterns we detected with MRI precede the reported window of NfL level changes by years. This temporal gap may be attributed to an initial subtle progression of neuronal damage at the earlier stages of disease, which does not result in detectable elevations of neurofilament levels. Unfortunately, no presymptomatic serum samples, which could have been used to determine NfL levels, were available for our phenoconverting subjects. To advance our understanding of the phenoconversion sequence to ALS or FTD, future efforts may include collecting blood samples from all (asymptomatic) participants at each MRI study visit.

The *C9orf72* repeat expansion is among the most common mutations found in ALS and FTD.[1,2] Recent research challenges initial beliefs of nearly complete penetrance at a late age[39], suggesting substantially lower estimates. The latest approximations of penetrance for ALS at age 80 stand at 24 to 44%.[4,5] Interestingly, our own predictions for *C9orf72* mutation carriers developing a phenoconverter endophenotype at age 80 (27.9%) closely resemble the recent approximations of penetrance in a large Dutch population-based cohort (28.7%),[4] although we used a fundamentally different approach.

By identifying a specific region prone to cortical atrophy in phenoconverters, we could explore distinguishing features within this area across all participant groups. This susceptible region, comprising mainly the frontal, temporal, and cingulate cortex, exhibited higher gyrification and thicker cortex than the rest of the brain, traits that are indicative of a more complex cortical structure.[40,41] This suggests that more complex cortical organization might be more vulnerable to damage, preluding atrophy in the process of phenoconversion to ALS-FTD, as demonstrated in other neurodegenerative disorders such as Huntington's disease and Alzheimer's disease.[34,42,43] Further investigation into the cellular, metabolic, and functional properties of these specific regions, compared to the rest of the brain, could provide valuable insights into understanding the underlying pathophysiological mechanisms in ALS-FTD. Cortical gyrification also serves as a marker for neurodevelopment.[8,44] Interestingly, although gyrification was reduced in all carriers of the *C9orf72* mutation, at approximately 40 years of age, it did not differ between non-converting AFM C9+ and presymptomatic phenoconverters, suggesting, in this regard, a comparable neurodevelopmental status at this point. Despite this similar neurodevelopmental status, presymptomatic phenoconverters still showed more cortical atrophy than other non-converting AFM C9+, supporting the idea that besides a *C9orf72* mutation, other potentially more individually determined factors contribute to the multistep process in the complex etiology of ALS-FTD.[45]

Longitudinally, cortical thinning in the phenoconverters showed a similar slope to that in non-converters, but started from a lower baseline, a trend also observed in subcortical volumes. In contrast, phenoconverters exhibited a progressively faster decline in gyrification compared to control groups, despite starting from a similar baseline. There are two potential explanations for the observed cortical thinning that our research cannot definitively distinguish: (1) phenoconverters may have experienced accelerated thinning earlier in life, slowing down because of reduced remaining cortex, or (2) they may have had a thinner cortex from the start, suggesting a neurodevelopmental issue. The more pronounced decrease in gyrification among phenoconverters may indicate an underlying neurodegenerative process, similar to what is observed in Alzheimer's and Huntington's diseases.[46–48] The exact mechanism behind this is unclear, but one possible explanation is that degeneration of subcortical structures leads to sulcal widening, resulting in a decrease in the gyrification index.

Investigating white matter connectivity in correlation to gyrification in phenoconverters may offer additional insights into impending phenoconversion to ALS or FTD.

Some limitations of our study should be acknowledged. First, given the rarity of capturing phenoconversion to diseases like ALS or ALS-FTD, our sample size of phenoconverters (n = 5) is limited, primarily drawn from family cohorts of ALS patients rather than FTD patients. Nonetheless, all five phenoconverters exhibit highly comparable patterns of atrophy with large effect sizes compared to the other subject groups, indicating a commonality among presymptomatic phenoconverters. Second, our focus solely on cerebral changes confines our conclusions regarding phenoconversion to ALS to upper motor neuron involvement in the brain. Consequently, potential lower motor neuron involvement in our presymptomatic phenoconverters and AFM C9+ group has not been captured. However, electrophysiological studies using the motor unit number index have reported that lower motor neuron loss occurs only a few months before weakness manifests.[49,50] Considering our detection of distinct brain abnormalities years before symptom onset, the impact of this exclusion is likely minimal. Nonetheless, future endeavors could benefit from integrating this neuroimaging research with other modalities, such as electromyography and neurofilament level measurements, to better understand the temporal order of changes in impending phenoconversion.

The ability to identify distinctive atrophy patterns in presymptomatic phenoconverters provides a potential new tool to quantify presymptomatic disease progression and to predict the timing of clinically manifest phenoconversion. For incomplete penetrant mutations, such as those associated with *C9orf72*, this approach might aid in the selection of trial participants and inform decisions regarding the necessity and timing of treatment initiation. To advance our comprehension and practical applications, continued research should focus on elucidating the fundamental biology of these common patterns, exploring their relationship with other biomarkers, and validating their predictive accuracy in other prospective cohorts.

Acknowledgments

This study received funding from the Netherlands ALS Foundation (Stichting ALS Nederland) and the European Research Council under the European Union's Horizon 2020 research and innovation program (grant agreement, 772376–EScORIAL). We thank all study participants for their valuable time and effort, both in sickness and in health.

Author Contributions

K.v.V., H.J.W., and L.H.v.d.B. contributed to the conception and design of the study; K.v.V., H.J.W., H.H.G.T., A.D.N., M.A.v.E., and J.H.V. contributed to the acquisition and analysis of data; K.v.V., H.J.W., and L.H.v.d.B. contributed to drafting the text or preparing the figures.

Potential Conflicts of Interest

Nothing to report.

Data Availability

The data supporting the findings of this study are available from the corresponding author, on reasonable request from qualified investigators, after permission from the appropriate regulatory authorities.

References

1. van Es MA, Hardiman O, Chio A, et al. Amyotrophic lateral sclerosis. Lancet 2017;390:2084–2098.
2. Grossman M, Seeley WW, Boxer AL, et al. Frontotemporal lobar degeneration. Nat Rev Dis Primers 2023;9:40.
3. Dharmadasa T, Scaber J, Edmond E, et al. Genetic testing in motor neurone disease. Pract Neurol 2022;22:107–116.
4. Van Wijk IF, Van Eijk RPA, Van Boxmeer L, et al. Assessment of risk of ALS conferred by the GGGGCC hexanucleotide repeat expansion in C9orf72 among first-degree relatives of patients with ALS carrying the repeat expansion. Amyotroph Lateral Scler Frontotemporal Degener 2024;25:188–196.
5. Spargo TP, Opie-Martin S, Bowles H, et al. Calculating variant penetrance from family history of disease and average family size in population-scale data. Genome Med 2022;14:141.
6. Mayl K, Shaw CE, Lee Y-B. Disease mechanisms and therapeutic approaches in C9orf72 ALS-FTD. Biomedicines 2021;9:601.
7. Benatar M, Turner MR, Wuu J. Presymptomatic amyotrophic lateral sclerosis: from characterization to prevention. Curr Opin Neurol 2023;36:360–364.
8. van Veenhuijzen K, Westeneng H-J, Tan HHG, et al. Longitudinal Effects of Asymptomatic C9orf72 Carriership on Brain Morphology. Ann Neurol 2023;93:668–680.
9. van Rheenen W, van Blitterswijk M, Huisman MHB, Vlam L, van Doormaal PTC, Seelen M, et al. Hexanucleotide repeat expansions in C9ORF72 in the spectrum of motor neuron diseases. Neurology 2012;79(9):878–882.
10. Costello E, Ryan M, Donohoe B, et al. Cognitive and neuropsychiatric endophenotypes in amyotrophic lateral sclerosis. Brain Commun 2023;5: fcad166.
11. Huisman MHB, de Jong SW, van Doormaal PTC, et al. Population based epidemiology of amyotrophic lateral sclerosis using capture-recapture methodology. J Neurol Neurosurg Psychiatry 2011;82: 1165–1170.
12. Nitert AD, Tan HHG, Walhout R, et al. Sensitivity of brain MRI and neurological examination for detection of upper motor neurone degeneration in amyotrophic lateral sclerosis. J Neurol Neurosurg Psychiatry 2022;93:82–92.
13. Brooks BR, Miller RG, Swash M, et al. El Escorial revisited: revised criteria for the diagnosis of amyotrophic lateral sclerosis. Amyotroph Lateral Scler Other Motor Neuron Disord 2000;1:293–299.

14. Rascovsky K, Hodges JR, Knopman D, et al. Sensitivity of revised diagnostic criteria for the behavioural variant of frontotemporal dementia. Brain 2011;134:2456–2477.

15. Walhout R, Schmidt R, Westeneng H-J, et al. Brain morphologic changes in asymptomatic C9orf72 repeat expansion carriers. Neurology 2015;85:1780–1788.

16. Iglesias JE, Insausti R, Lerma-Usabiaga G, et al. A probabilistic atlas of the human thalamic nuclei combining ex vivo MRI and histology. Neuroimage 2018;183:314–326.

17. Iglesias JE, Van Leemput K, Augustinack J, et al. Bayesian longitudinal segmentation of hippocampal substructures in brain MRI using subject-specific atlases. Neuroimage 2016;141:542–555.

18. Saygin ZM, Kliemann D, Iglesias JE, et al. High-resolution magnetic resonance imaging reveals nuclei of the human amygdala: manual segmentation to automatic atlas. Neuroimage 2017;155:370–382.

19. Bishop CM. *Pattern Recognition and Machine Learning*. New York, NY: Springer, 2006.

20. Smith SM, Nichols TE. Threshold-free cluster enhancement: addressing problems of smoothing, threshold dependence and localisation in cluster inference. Neuroimage 2009;44:83–98.

21. Yao AD, Cheng DL, Pan I, Kitamura F. Deep Learning in Neuroradiology: A Systematic Review of Current Algorithms and Approaches for the New Wave of Imaging Technology. Radiol Artif Intell 2020;2: e190026.

22. Kullback S, Leibler RA. On information and sufficiency. *Ann Math Stat*. 1951;22:79–86.

23. Cao B, Mwangi B, Passos IC, et al. Lifespan Gyrification Trajectories of Human Brain in Healthy Individuals and Patients with Major Psychiatric Disorders. Sci Rep 2017;7:511.

24. Popuri K, Dowds E, Beg MF, et al. Gray matter changes in asymptomatic C9orf72 and GRN mutation carriers. Neuroimage Clin 2018; 18:591–598.

25. Panman JL, Jiskoot LC, Bouts MJRJ, et al. Gray and white matter changes in presymptomatic genetic frontotemporal dementia: a longitudinal MRI study. Neurobiol Aging 2019;76:115–124.

26. Le Blanc G, Jetté Pomerleau V, McCarthy J, et al. Faster Cortical Thinning and Surface Area Loss in Presymptomatic and Symptomatic C9orf72 Repeat Expansion Adult Carriers. Ann Neurol 2020;88: 113–122.

27. Malpetti M, Jones PS, Tsvetanov KA, et al. Apathy in presymptomatic genetic frontotemporal dementia predicts cognitive decline and is driven by structural brain changes. Alzheimers Dement 2021;17:969–983.

28. Caverzasi E, Battistella G, Chu SA, et al. Gyrification abnormalities in presymptomatic c9orf72 expansion carriers. J Neurol Neurosurg Psychiatry 2019;90:1005–1010.

29. Rohrer JD, Nicholas JM, Cash DM, et al. Presymptomatic cognitive and neuroanatomical changes in genetic frontotemporal dementia in the Genetic Frontotemporal dementia Initiative (GENFI) study: a cross-sectional analysis. Lancet Neurol 2015;14:253–262.

30. Bocchetta M, Iglesias JE, Neason M, et al. Thalamic nuclei in frontotemporal dementia: Mediodorsal nucleus involvement is universal but pulvinar atrophy is unique to C9orf72. Hum Brain Mapp 2020;41:1006–1016.

31. Feis RA, Bouts MJRJ, de Vos F, et al. A multimodal MRI-based classification signature emerges just prior to symptom onset in frontotemporal dementia mutation carriers. J Neurol Neurosurg Psychiatry 2019;90:1207–1214.

32. Feis RA, van der Grond J, Bouts MJRJ, et al. Classification using fractional anisotropy predicts conversion in genetic frontotemporal dementia, a proof of concept. Brain Commun 2020;2: fcaa079.

33. Jiskoot LC, Panman JL, Meeter LH, et al. Longitudinal multimodal MRI as prognostic and diagnostic biomarker in presymptomatic familial frontotemporal dementia. Brain 2019;142:193–208.

34. Seeley WW, Crawford RK, Zhou J, et al. Neurodegenerative diseases target large-scale human brain networks. Neuron 2009;62:42–52.

35. Sedal L, Winkel A, Laing J, et al. Current concepts in multiple sclerosis therapy. Degener. Neurol. Neuromuscul. Dis. 2017;7:109–125.

36. Benatar M, Wuu J, Lombardi V, et al. Neurofilaments in presymptomatic ALS and the impact of genotype. Amyotroph Lateral Scler Frontotemporal Degener 2019;20:538–548.

37. Benatar M, Granit V, Andersen PM, et al. Mild motor impairment as prodromal state in amyotrophic lateral sclerosis: a new diagnostic entity. Brain 2022;145:3500–3508.

38. Staffaroni AM, Quintana M, Wendelberger B, et al. Temporal order of clinical and biomarker changes in familial frontotemporal dementia. Nat Med 2022;28:2194–2206.

39. Murphy NA, Arthur KC, Tienari PJ, et al. Age-related penetrance of the C9orf72 repeat expansion. Sci Rep 2017;7:2116.

40. la Fougère C, Grant S, Kostikov A, et al. Where in-vivo imaging meets cytoarchitectonics: the relationship between cortical thickness and neuronal density measured with high-resolution [18F]flumazenil-PET. Neuroimage 2011;56:951–960.

41. Wagstyl K, Larocque S, Cucurull G, et al. BigBrain 3D atlas of cortical layers: Cortical and laminar thickness gradients diverge in sensory and motor cortices. PLoS Biol 2020;18:e3000678.

42. Garcia-Gorro C, Llera A, Martinez-Horta S, et al. Specific patterns of brain alterations underlie distinct clinical profiles in Huntington's disease. Neuroimage Clin 2019;23:101900.

43. Pandya S, Maia PD, Freeze B, et al. Modeling seeding and neuroanatomic spread of pathology in amyotrophic lateral sclerosis. Neuroimage 2022;251:118968.

44. White T, Su S, Schmidt M, et al. The development of gyrification in childhood and adolescence. Brain Cogn 2010;72:36–45.

45. Chiò A, Mazzini L, D'Alfonso S, et al. The multistep hypothesis of ALS revisited: The role of genetic mutations. Neurology 2018;91: e635–e642.

46. Zhang Y, Fang T, Wang Y, et al. Occipital cortical gyrification reductions associate with decreased functional connectivity in amyotrophic lateral sclerosis. Brain Imaging Behav 2017;11:1–7.

47. Sterling NW, Wang M, Zhang L, et al. Stage-dependent loss of cortical gyrification as Parkinson disease "unfolds". Neurology 2016;86: 1143–1151.

48. Bachmann T, Schroeter ML, Chen K, et al. Longitudinal changes in surface based brain morphometry measures in amnestic mild cognitive impairment and Alzheimer's Disease. Neuroimage Clin 2023;38: 103371.

49. Neuwirth C, Barkhaus PE, Burkhardt C, et al. Motor Unit Number Index (MUNIX) detects motor neuron loss in pre-symptomatic muscles in Amyotrophic Lateral Sclerosis. Clin. Neurophysiol. 2017;128: 495–500.

50. Aggarwal A, Nicholson G. Detection of preclinical motor neurone loss in SOD1 mutation carriers using motor unit number estimation. J Neurol Neurosurg Psychiatry 2002;73:199–201.